

Article

One-Dimensional Computation Method of Supercritical CO₂ Labyrinth Seal

Yuming Zhu ^{1,2}, Yuyan Jiang ^{1,2,*}, Shiqiang Liang ^{1,2}, Chaohong Guo ^{1,2}, Yongxian Guo ¹ and Haofei Cai ^{1,2}

¹ Institute of Engineering Thermophysics, Chinese Academy of Sciences, 11 Beisihuanxi Rd, Beijing 100190, China; zhuyuming@iet.cn (Y.Z.); liangsq@iet.cn (S.L.); guochaohong@iet.cn (C.G.); guoyongxian@iet.cn (Y.G.); caihaofei@iet.cn (H.C.)

² School of Engineering Science, University of Chinese Academy of Sciences, No.19 (A) Yuquan Road, Shijingshan District, Beijing 100049, China

* Correspondence: yyjiang@iet.cn

Received: 11 July 2020; Accepted: 15 August 2020; Published: 20 August 2020

Abstract: An actual one-dimensional(1-D) computation method for a labyrinth seal is proposed. Relevant computation hypotheses for the 1-D method are analyzed and the specificity of internal flow in an SCO₂ (supercritical CO₂) labyrinth seal is explored in advance. Then, the experimental correlation discharge coefficient and the residual kinetic energy coefficient used in SCO₂ labyrinth seals are proposed. In addition, the speed of sound in two-phase flow is corrected in the 1-D method. All recent experimental results of the SCO₂ labyrinth seal are sorted out and the latest experimental results of a stepped-staggered labyrinth seal are proposed to verify the accuracy and applicability of the 1-D method. Finally, the sealing efficiency of the SCO₂ labyrinth seals are analyzed using the 1-D method.

Keywords: supercritical CO₂; labyrinth seal; 1-D computation; experiment

1. Introduction

At present, a large number of studies indicate that the supercritical CO₂(SCO₂) Brayton cycles may achieve much higher cycle efficiency than that of the Rankine cycle over a wide temperature range of heat sources with compact components, resulting in a significant decrease of generation costs [1–3]. The critical pressure of CO₂ is 7.38 MPa and the maximum pressure of a cycle may be up to 20 MPa, so the SCO₂ compressor's operational pressure is much higher than that of a traditional air compressor. Meanwhile, the viscosity of SCO₂ is close to that of air, and the density of SCO₂ is close to that of water, which may lead to a much thinner boundary layer and increase the leakage of the seal drastically. Hence, the leakage of SCO₂ in turbomachinery seals not only affects the cycle efficiency caused by parasitic losses, but also has paramount significance for evaluating the safety of the system under various working conditions [4].

The labyrinth seal, as one of the most commonly used non-contact seals, is widely employed in various rotary machines. There are different types of labyrinth seal, such as see-through, stepped, and staggered labyrinth seals. Haomin Yuan studied the see-through labyrinth seal used in SCO₂ flow both numerically and experimentally [5]. In the SNL (Sandia National Laboratory) SCO₂ Brayton cycle experiment loop, a stepped labyrinth seal was adopted for its compressor [6]. IET-CAS (Institute of Engineering Thermophysics, Chinese Academy of Sciences) developed a new kind of stepped-staggered labyrinth seal for its 1 MW SCO₂ compressor shaft end seal [7]. In terms of application, the labyrinth seals can be used as the major seal of the shaft end, the assisting seal of dry gas seals and the seal of the closed centrifugal impeller. Owing to the high power-density and the small size, tip clearance may lead to a serious decline in the performance, so the SCO₂ closed

centrifugal impeller is to have a higher efficiency than that of semi-open impeller [8]. This means that the SCO₂ labyrinth seal may be significant in the future design of high-performance SCO₂ compressors.

The labyrinth seal technology was firstly proposed by Parsons [9,10] to solve the sealing problems in steam turbines. Becker's study [11] first described the internal flow through the labyrinth in detail. Martin's formula (Equation (1)) is the first computation formula to predict the leakage flow rate through the labyrinth seal, which is based on an isothermal process with negligible velocity in chamber, and all velocities are to be under sonic velocity in his original work [12].

$$\dot{m} = CA \frac{P_0}{\sqrt{RT_0}} \sqrt{\frac{1 - \left(\frac{P_n}{P_0}\right)^2}{n - \ln\left(\frac{P_n}{P_0}\right)}} \quad (1)$$

where \dot{m} is the mass flow rate, kg/s, C is the flow discharge coefficient, A is the cross-sectional area of labyrinth seal, m², R is the ideal gas constant, P_0 is the upstream pressure, MPa, T_0 is the upstream temperature, K, P_n is the backpressure, MPa, and n is the teeth number.

Stodola assumed that the pressure drops at sealing teeth could be neglected, using Bernoulli's equation and the continuity equation [13]. Because it neglects the viscosity and compressibility of a fluid, it is only suitable for a small pressure difference on both sides of the sealing tooth or a large number of sealing teeth ($n > 4$). Egli's formula improves upon Martin's formula, and focuses on the impact of the kinetic energy transport effect on the seal. Therefore, a correction coefficient γ was defined. When γ is equal to 1, Egli's formula is reduced to Martin's formula [14]. Vermes's formula is still Martin's formula in form [15]. A non-adiabatic wall surface and the kinetic energy transport effect are modified by using an empirical coefficient which is based on boundary layer theory. Equation (2) is the Vermes formula of a see-through labyrinth seal.

$$\dot{m} = 5.67C \frac{A}{\sqrt{RT_0}} \frac{P_0}{\sqrt{1-\xi}} \beta, \quad \xi = \frac{8.52}{\frac{s-w}{c} + 7.23}, \quad \beta = \sqrt{\frac{1 - \left(\frac{P_n}{P_0}\right)^2}{n - \ln\left(\frac{P_n}{P_0}\right)}} \quad (2)$$

where \dot{m} is the mass flow rate, kg/s, C is the flow discharge coefficient, A is the cross-sectional area of labyrinth seal, m², R is the ideal gas constant, s is the length of sealing chamber, mm, w is the width of sealing tooth, mm, and c is the clearance at sealing tooth, mm. P_0 is the upstream pressure, MPa, T_0 is the upstream temperature, K, P_n is the backpressure, MPa, and n is the teeth number.

Gaotao Zhu proposed an iterative computation method, which applies to computation in both subcritical and critical working conditions [16].

However, all the above methods are based on the ideal gas thermodynamic process and can hardly satisfy the computation requirement of the labyrinth seal of the real fluid, in particular, supercritical fluid and two-phase fluid.

Recently, along with the application of SCO₂ becoming the research hot spot, some researchers are working towards establishing a computational model for the SCO₂ labyrinth seal. Fan et al. conducted an experimental study on the flow characteristics of the critical flow of SCO₂ under different single round hole structures, which can be seen as the single tooth labyrinth seal, and summarized empirical formulas (Equation (3)) [17]. Though the formulas are consistent with the single round hole experimental results, they are hardly used for the labyrinth's much more complex sealing structures. Additionally, the empirical formulas of nonlinear fitting applied for modifying the incompressible seal equation greatly limit the applicability of the model.

$$G = \left(0.5463 + 0.0587 \left(\frac{P_0}{P_{cr}} \right)^{2.07} \left(\frac{\rho_0}{\rho_{cr}} \right)^{-0.939} \right) \sqrt{2\rho_0(P_0 - P_c)} \quad (3)$$

where G is mass flow flux, kg/(m²s); P_0 is the upstream pressure, MPa; ρ_0 is the upstream density, kg/m³; P_{cr} is the critical pressure of CO₂, MPa; ρ_{cr} is the density at critical point of CO₂, kg/m³; P_c is the choked pressure, MPa.

Kim et al. modified the traditional computation theory by replacing 8.52 with 1.42 in Equation (2) according to the experimental data and obtained the computational model of the SCO₂ labyrinth seal, in which CO₂ was considered as an approximately ideal gas with a compression factor of 1, resulting in a huge computing error for the two-phase outlet conditions of the model [4]. Therefore, the model still needs to be further improved, because the outlet condition of the SCO₂ compressor major seals are mostly two-phase state.

Sandeep proposed an isentropic computational model of SCO₂ in his dissertation, and introduced a homogeneous flow model to enable the model to compute two-phase outlet conditions [18]. This model is essentially a zero-dimensional model that only considers the influence of inlet and outlet conditions and sealing clearance while neglecting that of the internal sealing structure.

In general, there is no accurate computational model that comprehensively considers both the physical property (including two-phase flow) changes and internal flow characteristics of the SCO₂ labyrinth seals. In this study, the flow is reasonably simplified and the equation of state of an ideal gas is not required for the whole calculation, which means that there is no need to correct the model for the compressibility of SCO₂, so the relevant empirical coefficients in the one-dimensional(1-D) method, including flow discharge coefficient and kinetic residual coefficient, can be more universally applicable. In addition, the homogeneous two-phase flow model is introduced, and some essential computational parameters are modified so that the model can also compute the two-phase outlet conditions.

Recent experimental results of the SCO₂ labyrinth seal are sorted out in this article and the latest results of the SCO₂ stepped–staggered labyrinth seal is proposed. The 1-D computation method is verified with the experimental results of different types of labyrinth seal, such as round-hole, see-through, and stepped-staggered SCO₂ labyrinth seals. Finally, the essential sealing performance of the SCO₂ labyrinth seals is studied using the 1-D method.

2. 1-D Computation Method

In this section, the 1-D computation method of labyrinth seals is discussed based on the essential structure of the labyrinth seals as is shown in Figure 1. s and h are the length and height of sealing chamber, respectively, w is the width of sealing tooth, c is the clearance at sealing tooth, r is the radius of sealing shaft, and u is the axial velocity of leakage flow.

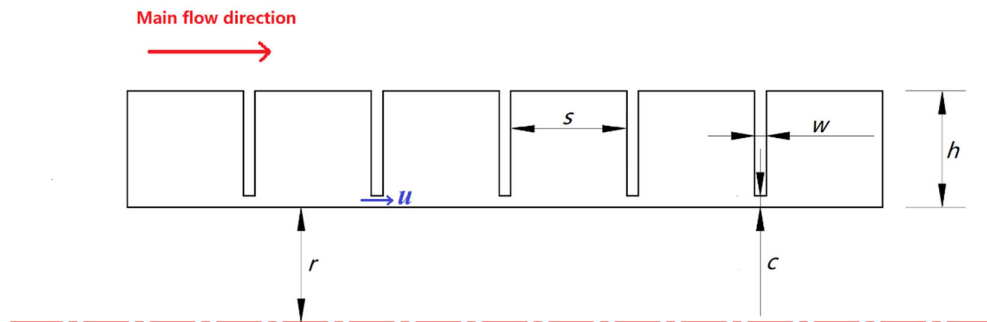


Figure 1. The essential structure of the labyrinth seal.

2.1. Computation Hypotheses

2.1.1. 1-D Flow Hypothesis

Figure 2 shows the steady-state streamlines diagram of the SCO₂ see-through labyrinth seal, in which the red and the blue streamlines represent the main and whirling flows in sealing chambers, respectively. Although the internal flow of the labyrinth seal is complex and has lots of vortices, the main flow has an obvious 1-D flow characteristics and directly determines the seal leakage. The impact of the vortex flow can be considered as a correction coefficient, namely the residual kinetic energy coefficient θ . In addition, it is well known that the distribution of velocity at labyrinth tooth is far from 1-D, especially under the influence of a boundary layer, the heterogeneity of leakage flow in the 1-D model is corrected by flow discharge coefficient C .

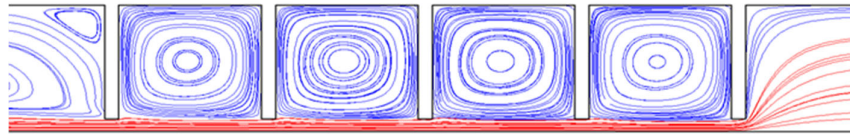


Figure 2. Steady-state streamline of a supercritical CO₂ see-through labyrinth seal.

The 1-D flow needs to be discretized to facilitate the model. As for the leakage flow at sealing teeth, the flow experiences a process of expansion. There must be a point where the axial velocity reaches maximum and the static pressure reaches minimum, and this point is used as the computational site of the sealing teeth. For the leakage flow at sealing chambers, the main flow is decelerated by the whirling motion in sealing chambers. There must be a point where the axial velocity reaches minimum, and this point is used as the computational site of the sealing chambers. Then, the sealing chambers are represented by 0 to n and the sealing teeth are represented by 0.5 to $n - 0.5$. See Figure 3 for details.

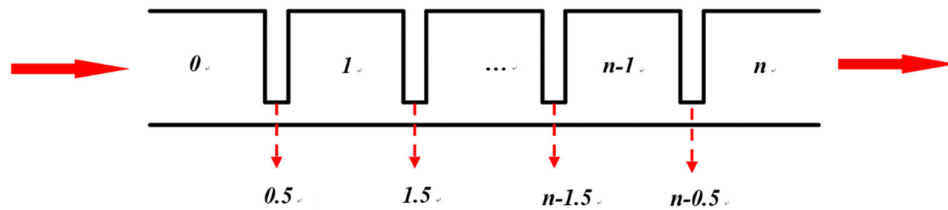


Figure 3. 1-D computation site distribution of labyrinth seal.

2.1.2. Governing Equation

For the overall sealing process, it follows two governing equations: the continuity equation and the energy equation.

The continuity equation:

$$\dot{m}(0) = \dot{m}(0.5) = \dot{m}(1) = \dot{m}(1.5) = \dots = \dot{m}(n-1.5) = \dot{m}(n-1) = \dot{m}(n-0.5) = \dot{m}(n) \quad (4)$$

where \dot{m} is the mass flow rate, kg/s.

The energy equation:

$$h_0(1) = h_0(0.5) = h_0(1) = h_0(1.5) = \dots = h_0(n-1.5) = h_0(n-1) = h_0(n-0.5) = h_0(n) \quad (5)$$

$$h_0 = h + k \quad (6)$$

$$k = \frac{u^2}{2} \quad (7)$$

As is shown in Equations (5)–(7), h_0 is the total enthalpy, J/kg; k is defined as the unit kinetic energy of the 1-D flow, J/kg; u is the axial velocity, m/s.

2.2. Computational Process

2.2.1. Isentropic Expansion Process

The isentropic expansion process needs to follow two governing equations in Section 2.1.2 and satisfy the isentropic expansion thermodynamic process equation at the same time. During computation of the mass flow at the sealing teeth, an estimation formula of the flow discharge coefficient C needs to be provided based on experimental or numerical simulation results of different sealing structures and working fluids. It is defined as follows:

$$C = \frac{\bar{u}}{u} \quad (8)$$

In Equation (8), \bar{u} is the average axial velocity at tooth, m/s; u is the axial velocity at tooth calculated by isentropic process, m/s.

The governing equations of the isentropic expansion process are as follows:

$$\begin{cases} s(n-1) = s(n-0.5) \\ h_0(n-1) = h(n-0.5) + k(n-0.5) = h_{00} \\ \dot{m}(n-0.5) = C(n-0.5) * \rho(n-0.5) * u(n-0.5) * A(n-0.5) = \dot{m}_{00} \end{cases} \quad (9)$$

where h_{00} is the initial total enthalpy, J/kg; s is the entropy, kJ/(kg·K); A is the cross-sectional area of labyrinth seal, m²;

The isentropic expansion process requires iterative computation. The purpose of iteration is to adjust the pressure difference of the seal, so that the computed seal leakage is equal to an expected leakage. Moreover, the specific iteration process is as follows:

- i. The expected mass flow \dot{m}_{00} is provided for computation of labyrinth seal performance;
- ii. For the computation site $n - 0.5$, $P(n - 1)$ has been obtained, and an initial static pressure difference δP is provided. In this case, $P(n - 0.5)$ is determined.
- iii. $s(n - 0.5)$ is obtained from the governing equation $s(n - 1) = s(n - 0.5)$. Using (P, s) to query the National Institute of Standards and Technology (NIST) reference fluid thermodynamic and transport properties database (REFPROP) [19], the thermodynamic states (T, h, p, \dots) at $n - 0.5$ can be obtained.
- iv. Based on the total enthalpy conservation, the unit kinetic energy $k(n - 0.5)$ at $n - 0.5$ is computed, and then the flow velocity at $n - 0.5$ is obtained. The mass flow $\dot{m}(n - 0.5)$ is computed and compared with the expected mass flow \dot{m}_{00} . If $\dot{m}(n - 0.5)$ is smaller, the static pressure is increased by the pressure difference δP ; or if $\dot{m}(n - 0.5)$ is larger, the provided static is reduced by the pressure difference δP .
- v. Iteration is performed under the error between $\dot{m}(n - 0.5)$ and \dot{m}_{00} is within the iterative error $\delta \dot{m}$ ($\delta \dot{m} = 0.002$ kg/s in this study). End the iteration process and enter the computation process of the computational site $n - 0.5$ to n .

2.2.2. Isobaric Dissipation Process

The kinetic energy transport effect occurs in the isobaric dissipation process, and has great impact on labyrinth seal performance. Therefore, an empirical coefficient used to measure the kinetic energy transport effect is one of the essential parameters to evaluate the labyrinth seal. For the ideal

labyrinth sealing process, all unit kinetic energy $k(n - 0.5)$ of the main flow that is expanded by the sealing teeth $n - 0.5$ is dissipated by the vortex flow in the sealing chamber n , and the residual kinetic energy coefficient is θ . However, the kinetic energy of the main flow is not dissipated completely, and the residual kinetic energy coefficient differs along with different seal forms or different working fluids in the real sealing process. In this study, the unit kinetic energy k of the main flow is used to represent the residual kinetic energy coefficient θ to measure the kinetic energy transport effect, which is defined as follows:

$$\theta = \frac{k(n)}{k(n-0.5)} = \frac{\frac{u^2(n)}{2}}{\frac{u^2(n-0.5)}{2}} \quad (10)$$

The governing system of the isobaric dissipation process are as follows:

$$\begin{cases} P(n-0.5) = P(n) \\ k(n) = \theta(n) \cdot k(n-0.5) \\ h(n) + k(n) = h_{00} \end{cases} \quad (11)$$

Using computational fluid dynamics (CFD) or experimental data, the estimation formula of the residual kinetic energy coefficient θ is sorted out, and the static enthalpy $h(n)$ in the sealing chamber is computed. The thermodynamic state (T, h, p, \dots) in the sealing chamber n can be obtained by inquiring the NIST physical property database of a real fluid with (P, h).

2.2.3. Overall Performance Computation of Labyrinth Seal

After completing the iteration computation from the computational site $n - 1$ to $n - 0.5$ and the computational site computation from $n - 0.5$ to n , the computation process of a sealing unit (including a sealing chamber and tooth) is completed. If there is a sealing tooth $n+0.5$ behind the sealing chamber n , the computation processes listed in Sections 2.2.1 and 2.2.2 are repeated until computations of all sealing units are completed. An outlet pressure of the last sealing unit is P_{out} . Then, for a given expected flow \dot{m}_{00} , the pressure ratio of the labyrinth seal is P_{out}/P_0 .

The critical flow, also called “choked” flow, is a limiting condition which occurs when the mass flow rate will not increase with a further decrease in the downstream pressure environment while upstream pressure is fixed. For homogeneous fluids, the physical point at which the choking occurs for adiabatic conditions is when the exit velocity is at sonic conditions or at a Mach number of 1. So, in the 1-D computational method, the critical flow condition is judged by the local Mach number $Ma(i) = u(i)/a(i)$ at a certain computational site i reaching 1, where the $u(i)$ is the axial velocity and $a(i)$ is the speed of sound at computational site i . As the \dot{m}_{00} increases, the local Mach number $Ma(i)$ gradually increase. As the local Mach number $Ma(i)$ reaches 1, the iteration process of the overall performance calculation of labyrinth seal is finished.

Besides, for the requirement of accurate calculation of critical flow in SCO_2 labyrinth seals, the flow discharge coefficient C under critical condition may increase as backpressure decreases, which is available in Section 3.1.2.

Figure 4 shows a basic block diagram of the 1-D computation process of the labyrinth seal.

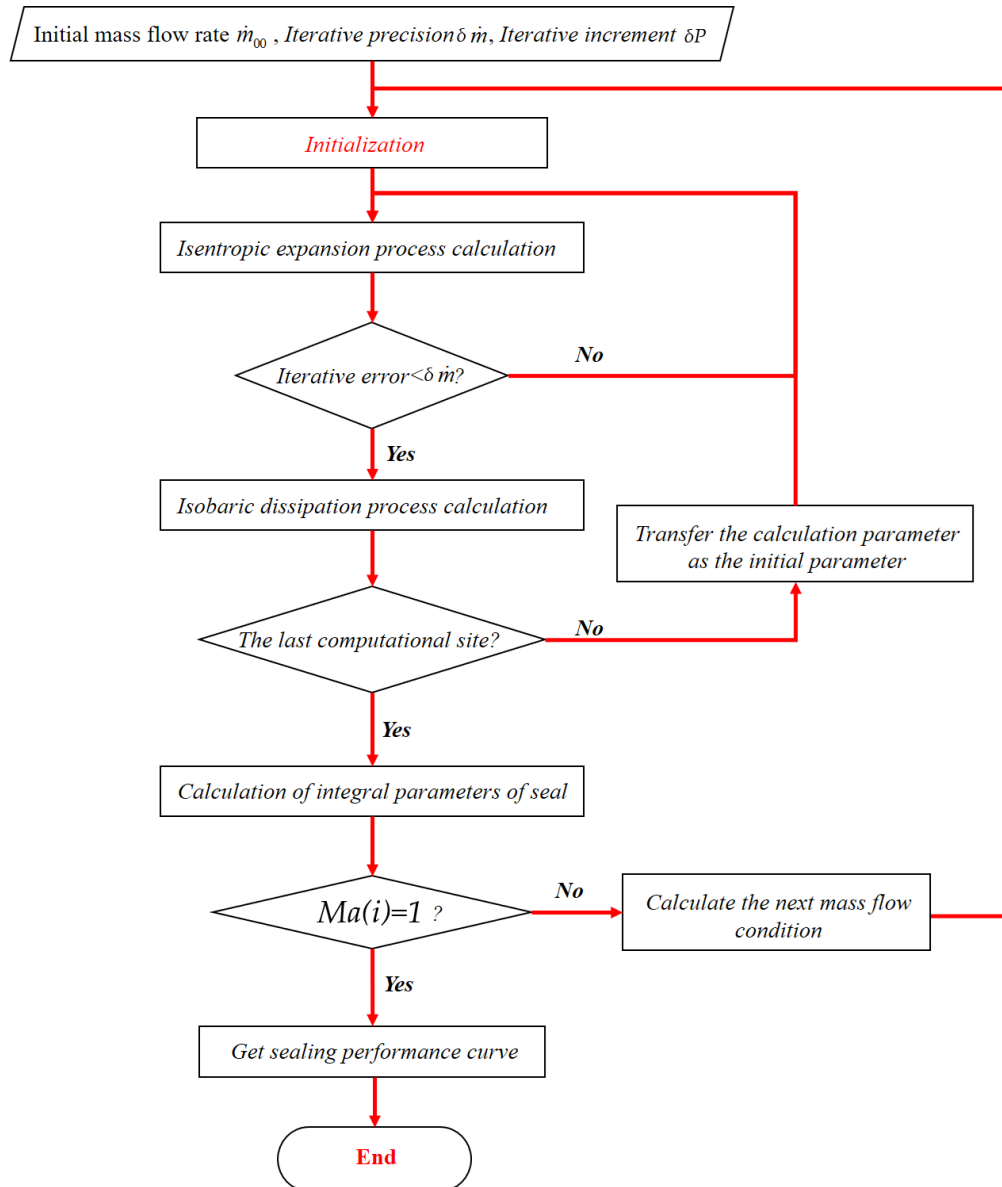


Figure 4. Block diagram of one-dimensional(1-D) computation process of labyrinth seal.

3. Internal Flow Property of SCO₂ Labyrinth Seal

Section 2 introduces a 1-D computation method that comprises two characteristic parameters: flow discharge coefficient C and residual kinetic energy coefficient θ . The effects of different sealing fluids and geometrical structures on the performance of the labyrinth seal are reflected by C and θ in the 1-D computation. At present, there are few studies on the characteristic parameters of the labyrinth seal with SCO₂ as the working fluids. This section analyzes the particularity of leakage flow and tries to provide the correlation of flow discharge coefficient C and residual kinetic energy coefficient θ in the SCO₂ labyrinth seal.

In this section, the see-through labyrinth seal structure (as shown in Figure 5) given in reference [5] is considered as a reference object. Through the study of the numerical simulation of an internal flow field of the SCO₂ labyrinth seal, the internal flow property of the SCO₂ labyrinth seal is explored in advance. The details of the numerical method were described in reference [7], which was verified by the experimental method. Further, to compare the difference of SCO₂ and air flow in the labyrinth seal, the numerical study of air is conducted, and it has the same pressure ratio as that of SCO₂. Table 1 lists the inlet and outlet boundary conditions of the numerical simulation.

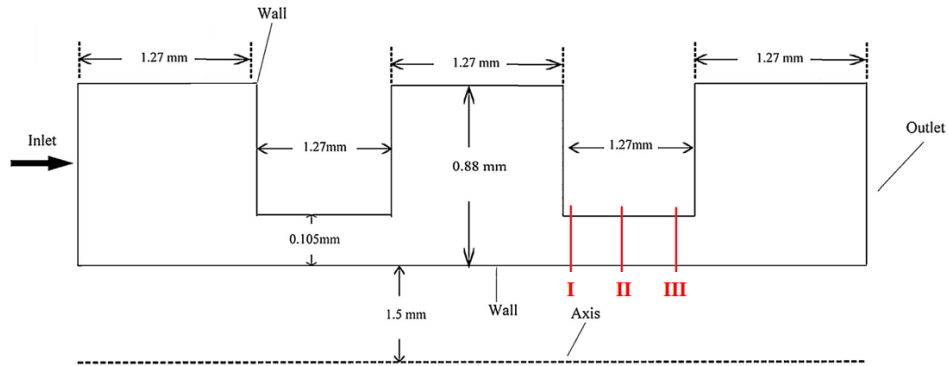


Figure 5. The structure of see-through labyrinth seal used in Yuan’s experiment.

Table 1. The inlet & outlet boundary condition of numerical simulation.

	Inlet Pressure (MPa)	Inlet Temperature (K)	Outlet Pressure (MPa)
SCO ₂	10	320	7
Air	0.143	273	0.1

3.1. Flow Discharge Coefficient C of SCO₂ Labyrinth Seal

3.1.1. Particularity of Flow Discharge Coefficient in SCO₂ Labyrinth Seal

As summarized in Table 2, viscosity of SCO₂ is close to that of air, and the density of SCO₂ is about 400 times higher. Based on the see-through labyrinth seal in Figure 5 and the definition of Reynolds (*Re*) number at sealing teeth (Equation (12)), Table 2 tries to compare *Re* number at the second sealing teeth of SCO₂ and air as working fluid. The *Re* number of SCO₂ flow is over 10⁵, and it is turbulent flow, but the air flow has a *Re* number less than 2300 and is basically laminar flow. The internal flow velocity profiles of the two kinds of flows are different. The laminar flow follows a quadratic parabolic velocity distribution, while the turbulence flow follows the power exponential distribution, especially when the *Re* number is about 10⁵ and the power index is 1/7, known as the Karman–Prandtl’s 1/7th power law, and it was proven by Nikuradse through experiment. So, the turbulent flow has a higher average axial velocity, and it can be expected that the SCO₂ labyrinth seals have a higher flow discharge coefficient than that of air labyrinth seals.

$$Re = \frac{\rho uc}{\mu} \tag{12}$$

Table 2. *Re* number at the second sealing teeth of SCO₂ and air as working fluid.

	<i>u</i>	ρ	μ	<i>c</i>	<i>Re</i>
	m/s	kg/m ³	10 ⁻⁵ Pa·s	mm	-
SCO ₂	90	448	3.2	0.105	132,000
Air	140	1.18	1.8	0.105	964

Based on the Equation (8), the numerical results of the flow discharge coefficient at position I–III (shown in Figure 5) of the SCO₂ labyrinth seal are listed in Table 3. Overall, the flow discharge coefficient of the SCO₂ working fluid is 15–30% larger than that of the air working fluid.

Table 3. Flow discharge coefficient of SCO₂ and air at different positions.

	Position I	Position II	Position III
SCO ₂	0.718	0.786	0.862
Air	0.68	0.67	0.66

3.1.2. The Correlation of Flow Discharge Coefficient C in SCO₂ Labyrinth Seal

Suryanarayanan et al. carried out a detailed study on the flow discharge coefficient of traditional labyrinth seals and obtained the experimental correlation (Equation (13)), in which the application range is $250 < Re < 15,000$, and Equation (13) is much more suitable for incompressible fluids, including water and air at a high pressure ratio [20].

$$C = \frac{0.7757 - 0.002051 \left(\frac{w}{c}\right)}{\left(1 + \frac{44.86 \left(\frac{w}{c}\right)}{Re}\right)^{0.2157}} \tag{13}$$

Though this equation cannot be directly used for the SCO₂ labyrinth seal for its extremely high *Re* number, as shown in Table 2, it can be expected that the *C* of SCO₂ labyrinth seals may have a similar form as Equation (13). Furuichi et al. investigated the discharge coefficient *C* of nozzle in high *Re* number, and It was found that the growth rate of discharge coefficient *C* is less than 2% when the *Re* number increases from 10⁵ to 10⁷ [21], which may be suitable for SCO₂ labyrinth seals with the same *Re* number range. Besides, it is difficult to consider the impact of all factors for the experimental data of SCO₂ labyrinth seal is limited. So, it is logical to ignore the influence of *Re* number on the flow discharge coefficient *C* when the *Re* number is 10⁵–10⁷. Considering the *Re* number of SCO₂ labyrinth seals is far less than 10⁷, the criterion, $Re > 1 \times 10^5$, should be carefully checked when the 1-D method is used.

Kim’s single round-hole leakage experiment used a high-pressure tank as the upstream and used a low-pressure tank as the downstream [4]. The initial condition of high-pressure tank is 13.5 MPa and 160 °C and the initial condition of low-pressure tank is normal temperature and pressure. As the valve between high-pressure tank and low-pressure tank is opened, the huge pressure difference causes critical flow in the beginning. As the pressure of different tanks gradually balances, the leakage flow turns into non-critical flow in the end and the whole experiment lasted about 210 s as is shown in Figure 6. The mass flux was obtained by calculating the mass difference of the tank for every second. So, the uncertainty is severely affected by the measure of temperature and pressure, which leads to an average uncertainty of ±3694.7 kg/m². Applying the definition of *C* to analyze the experimental results in Figure 6, the variation curve of *C* with pressure ratio can be obtained in Figure 7. The *C* increases with the decrease of the pressure ratio when the leakage flow is under critical condition (pressure ratio < 0.6), and *C* basically keeps unchanged on the area of non-critical flow. The experimental results indicated that when outlet pressure is equivalent to atmospheric pressure, the critical pressure ratio at the outlet reaches the maximum, so does the flow discharge coefficient *C*. The single round-hole has the diameter (*c*) of 1.5 mm and length (*w*) of 5.0 mm, so the *w/c* is 10/3 and a preliminary experimental correlation of *C* can be obtained, as is shown in Equation (14), which may not be very accurate due to the uncertainty of measurement.

$$C = \begin{cases} 0.96 - 0.08 \left(\frac{P_{out}}{P_c}\right), & \frac{P_{out}}{P_c} \leq 1 \\ 0.88, & \frac{P_{out}}{P_c} > 1 \end{cases}, \frac{w}{c} = \frac{10}{3} \tag{14}$$

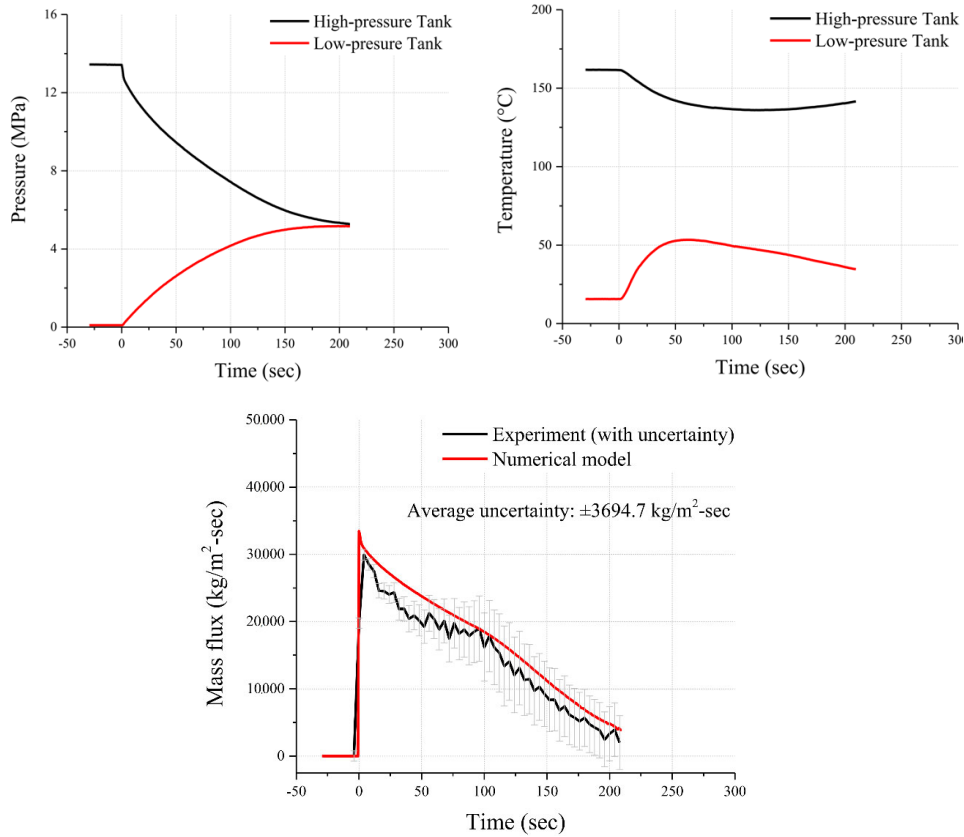


Figure 6. The single round-hole leakage experiment results given by Kim.

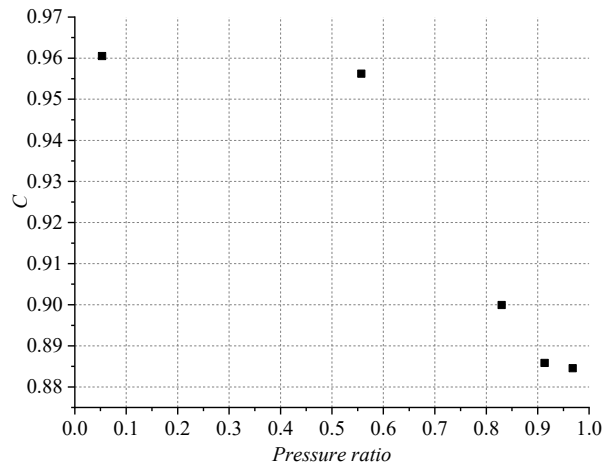


Figure 7. The variation curve of C with pressure ratio based on Kim’s experiment.

Fan experimented on SCO_2 critical leakage flow of single round-hole with different structures, in which the outlet pressure is atmospheric pressure and P_{out}/P_c is close to 0, and the critical discharge flow coefficient is maximum under this condition [17]. Table 4 shows the operation condition and results where w is the length of single round-hole and c is the diameter of single round-hole. Then, the experimental results of different w/c were further processed to obtain the variation curve of the maximum critical C with w/c (Figure 8). As w/c increases, the maximum critical C decreases but remains unchanged between 0.9 and 0.91 when w/c is more than 5. Then, the correlation of maximum critical C can be concluded as Equation (15).

$$\text{The maximum critical } C = \begin{cases} 1 - 0.023\left(\frac{w}{c}\right)^{0.875}, \frac{w}{c} \leq 5, \frac{P_{out}}{P_c} \approx 0 \\ 0.9059, \frac{w}{c} > 5 \end{cases} \quad (15)$$

Table 4. The results of single round-hole with different w/c .

w/c	Inlet Pressure (MPa)	Inlet Temperature (°C)	Mass Flow Rate (kg/h)	Maximum Critical C
1	9.98	49.4	113.8	0.974
3	9.98	49.4	110.8	0.948
5	10.17	50.1	108.9	0.917
8	10.04	50.1	104.9	0.903
10	9.97	50.7	104.0	0.908
15	9.93	50.9	103.5	0.914

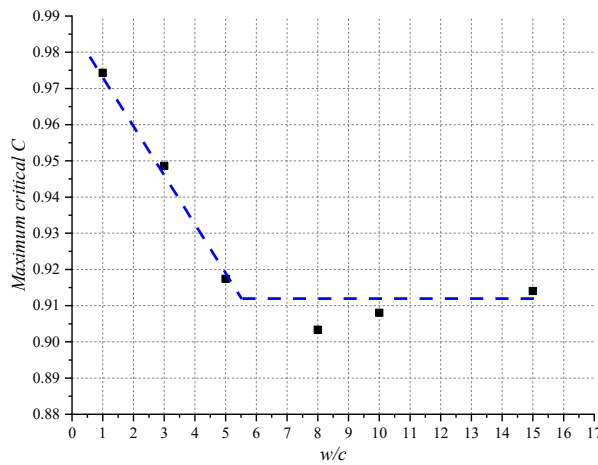


Figure 8. The variation curve of maximum critical C with w/c based on Fan’s experiment.

Equation (14) describes the change rule of flow discharge coefficient C with the pressure ratio and Equation (15) describes the change rule of maximum critical C with w/c . However, neither Equation (14) nor Equation (15) can represent the complete correlation of the flow discharge coefficient C. Combining and extending the Equation (14) and Equation (15), the preliminary correlation of flow discharge coefficient C for SCO₂ labyrinth seals is proposed in Equation (16).

$$C = \begin{cases} 1 - 0.023\left(\frac{w}{c}\right)^{0.875} - 0.085\left(\frac{P_{out}}{P_c}\right), \frac{w}{c} \leq 5, \frac{P_{out}}{P_c} \leq 1 \\ 0.9059 - 0.085\left(\frac{P_{out}}{P_c}\right), \frac{w}{c} > 5, \frac{P_{out}}{P_c} \leq 1 \\ 0.915 - 0.023\left(\frac{w}{c}\right)^{0.875}, \frac{w}{c} \leq 5, \frac{P_{out}}{P_c} > 1 \\ 0.82, \frac{w}{c} > 5, \frac{P_{out}}{P_c} > 1 \end{cases} \quad (16)$$

3.2. Residual Kinetic Energy Coefficient θ of SCO_2 Labyrinth Seal

3.2.1. Particularity of Residual Kinetic Energy Coefficient θ of SCO_2 Labyrinth Seal

Based on the numerical of the see-through labyrinth seals in Figure 5, the streamline diagrams of the middle sealing chamber using SCO_2 and air as working fluids are shown in Figure 9 and Figure 10 respectively. Compared with the air flow, the SCO_2 flow has smaller viscosity, higher density, and larger inertia. As a result, the expansion effect of the SCO_2 main flow is weak and the vortex flow has a smaller number of vortices. It can be found that the expansion angle of the SCO_2 main flow is smaller and the kinetic energy transport effect is more obvious, so the residual kinetic energy coefficient θ of the SCO_2 labyrinth seal may be higher than that of the air labyrinth seal.

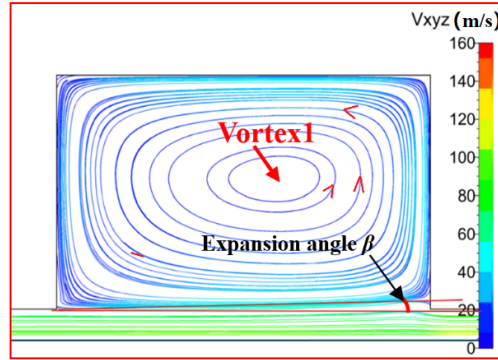


Figure 9. Internal streamline of SCO_2 as working fluid.

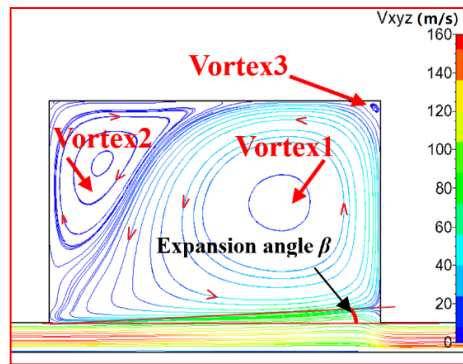


Figure 10. Internal streamline of air as working fluid.

Based on the definition of θ in Equation (10), it can be computed for the middle sealing chamber. The results of SCO_2 and air flow at the middle sealing chamber are summarized in Table 5. θ value for the SCO_2 is about 0.76 and that of air is keep at 0.53. It is worthy of note that the maximum of θ is 1, which means that no kinetic energy loss occurred in the sealing chamber, and the leakage is maximum. When the minimum of θ is 0, which means that all kinetic energy in the seal chamber is dissipated, the leakage is minimum. Further, Table 5 shows that SCO_2 is much more difficult to be sealed in the industrial application.

Table 5. Residual kinetic energy coefficient θ of SCO_2 and air flow at middle sealing chamber.

θ (Middle Sealing Chamber)	
SCO_2	0.76
Air	0.53

3.2.2. The Experimental Correlation of Kinetic Residual Coefficient θ

The traditional kinetic transport coefficient is essentially the correction coefficient of leakage flow, which cannot directly reflect the internal flow of labyrinth seals. The kinetic residual coefficient is used to characterize the dissipation effect of mainstream flow in the seal chamber in this paper, which is of direct physical significance and can better demonstrate the physical essence of the flow in sealing chambers. Nevertheless, the phenomenon described by the traditional kinetic transport coefficient is identical with the kinetic residual coefficient used in this paper, so the main influencing factors and the basic form of the empirical equation should be consistent, as is shown in Equation (17) [22].

$$\gamma = \left(1 - 6.5 \left(\frac{c}{s}\right)\right) \left(Re + \left(1 - 6.5 \left(\frac{c}{s}\right)\right)^{\frac{-1}{2.454 \left(\frac{c}{s}\right)}} \right)^{2.454 \left(\frac{c}{s}\right)} \quad (17)$$

According to Sandeep, c/s is the main influencing factor of kinetic transport coefficient [18]. Due to the limited experimental data, the kinetic residual coefficient is employed for c/s fitting in this paper. The influence of w/c and h/c will be further considered in the subsequent research.

Compared with the flow discharge coefficient, the kinetic residual coefficient is hard to measure and the experimental results of SCO_2 are very limited. In this section, the kinetic energy residual coefficient is not analyzed in detail, the primary values of the kinetic energy residual coefficient in SCO_2 labyrinth seals are given in Equation (18). The kinetic residual coefficient θ for round-hole and see-through labyrinth seals is obtained by the CFD results in reference [5] and θ for staggered labyrinth seals is obtained by the CFD results in reference [7]. Despite this, Equation (18) has a certain application value considering that there is seldom a correlation of the kinetic residual coefficient θ for SCO_2 labyrinth seals and this will be verified by the available experimental results in Section 4.1.

$$\theta = \begin{cases} 1 - 0.04696 \left(\frac{s}{c}\right)^{0.6745}, & \text{round-hole and see-through labyrinth seals} \\ 0.12, & \text{staggered labyrinth seals} \end{cases} \quad (18)$$

3.3. Two-Phase Critical Flow in SCO_2 Labyrinth Seal

Two-phase and critical flow is one of the typical characteristics of SCO_2 labyrinth seal and it is paramount for the 1-D method to capture the position of the two-phase critical flow. Applying the isentropic model to calculate the two-phase critical flow. The curve of sealing performance of round hole is shown in Figure 11 and Table 6, and the round hole structure of Fan's experiment in Table 7 is used and the upstream condition is 10 MPa and 323 K [17]. As the outlet pressure decreases, the mass flow rate attains a peak at 7 MPa where the Ma number is just 0.73. This means that the Ma number at the maximum isentropic leakage point has not reached 1.

Table 6. The sealing performance of round hole calculated by 1-D method.

P_{out}	Mass Flow Rate	Ma	Speed of Sound
MPa	kg/h		m/s
10.00	0.00	0.00	218.09
9.80	34.86	0.15	215.74
9.60	48.88	0.21	213.33
9.40	59.33	0.27	210.84
9.20	67.87	0.31	208.29
9.00	75.15	0.35	205.66
8.80	81.50	0.39	202.97
8.60	87.11	0.43	200.25
8.40	92.10	0.47	197.51
8.20	96.56	0.51	194.77
8.00	100.56	0.55	192.05
7.80	104.14	0.58	189.35
7.60	107.33	0.62	186.62
7.40	110.16	0.66	183.79
7.20	112.63	0.70	180.76
7.00	114.22(max)	0.73 < 1	179.11
6.80	113.90	0.75	181.31
6.60	113.49	0.77	182.42
6.40	112.94	0.80	183.00
6.20	112.24	0.82	183.27
6.10	111.83	0.84	183.34
6.00	111.39	0.85	183.38

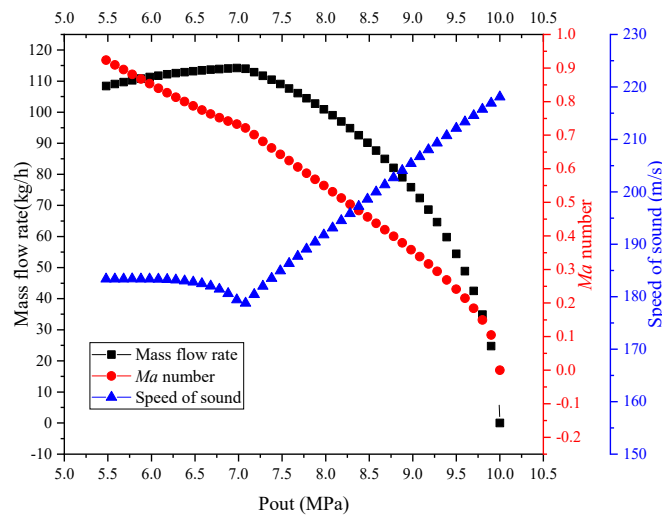


Figure 11. The curve of sealing performance of round hole calculated by 1-D method.

According to the definition of the Ma number in Section 2.2.3 and the deduction process of the two-phase speed of sound $a_{Two-phase}$ shown Equation (19), the vital point for the computation of two-phase flow Ma number is the accuracy of a_v and a_l which is defined by the isentropic change of $\frac{\partial P}{\partial \rho}$.

$$\begin{aligned}
 a_{two-phase} &= \left(\frac{\partial P}{\partial \rho} \right)_s = \left(\frac{\partial \rho}{\partial P} \right)_s^{-1} = \left(\frac{\partial v}{\partial P} \cdot \left(-\frac{1}{v^2} \right) \right)_s^{-1} \\
 &= \left(\frac{\partial (x_g v_g + (1-x_g)v_l)}{\partial P} \cdot \left(-\frac{1}{v^2} \right) \right)_s^{-1} \\
 &= \left(\left(x_g \left(\frac{\partial v_g}{\partial P} \right)_{s_g} + (1-x_g) \left(\frac{\partial v_l}{\partial P} \right)_{s_l} \right) \cdot \left(-\frac{1}{v^2} \right) \right)_s^{-1} \\
 &= \left(\rho^2 \left(\frac{x_g}{(a_g \rho_g)^2} + \frac{1-x_g}{(a_l \rho_l)^2} \right) \right)_s^{-1}, s = x_g s_g + (1-x_g) s_l \\
 a_g &= \left(\frac{\partial P}{\partial \rho_g} \right)_{s_g}, a_l = \left(\frac{\partial P}{\partial \rho_l} \right)_{s_l}
 \end{aligned} \tag{19}$$

where the subscripts s represents the isentropic process of two-phase flow. The subscripts s_g represents the isentropic process of saturated gas. The subscripts s_l represents the isentropic process of saturated liquid; v is the specific volume of two-phase flow; ρ_g and ρ_l are the density of saturated gas and saturated liquid respectively; a_g and a_l are the speed of sound of saturated gas and saturated liquid respectively; x_g is the dryness of two-phase flow, which represents the mass fraction of saturated gas.

The isentropic model is used to calculate the curve of density with a change of outlet pressure and inlet temperature (290 K–340 K) in which the inlet pressure is unchanged at 10 MPa. It can be found in Figure 12 that when the outlet condition enters the two-phase region, the change rate of density decreases suddenly. According to the definition of two-phase speed of sound $a_{two-phase}$ in Equation (19), the sudden change of speed of sound will occur when the outlet flow enters the two-phase condition. Also, as the inlet temperature decreases, the sudden change becomes much more obvious.

The original 1-D method uses the a_v and a_l provided by NIST physical property model, and it may lead to the problem of two-phase critical flow. Using the Figure 12 to further discuss the speed of sound of a_v and a_l , the dotted line represents the saturation line. Considering the definition of the speed of sound in Equation (19), $\left(\frac{\partial P}{\partial \rho} \right)_s$ does not exist at the saturation line, because the left-hand partial derivative of $\left(\frac{\partial P}{\partial \rho} \right)_s$ is not equal to the right-hand partial derivative of $\left(\frac{\partial P}{\partial \rho} \right)_s$. For the condensation process, both density and pressure decrease along the direction of flow, so the actual formula of a_v and a_l is the right-hand partial derivative of $\left(\frac{\partial P}{\partial \rho} \right)_s$. However, the a_v and a_l provided by the NIST database is the left-hand partial derivative of $\left(\frac{\partial P}{\partial \rho} \right)_s$ which is larger than the correct value, and it leads to the calculated error of the Ma number.

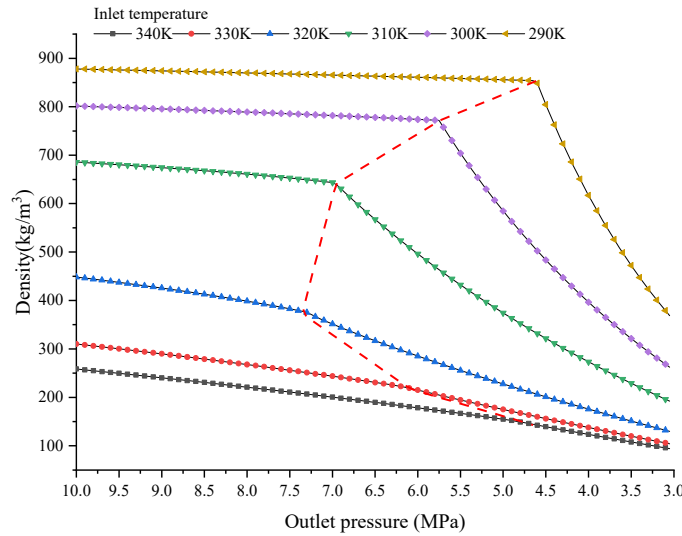


Figure 12. Curve of density with change of outlet pressure and inlet temperature using isentropic model.

Correcting the 1-D method by replacing the a_v and a_l by right-hand partial derivative of $\left(\frac{\partial P}{\partial \rho}\right)_s$, Figure 13 shows that the mass flow rate attains the maximum at the position of $Ma = 1$, which is consistent with the definition of critical flow in Section 2.2.3. Therefore, using the NIST physical property model and homogeneous two-phase model to calculate the two-phase flow, the speed of sound of a_v and a_l should be corrected in the 1-D method.

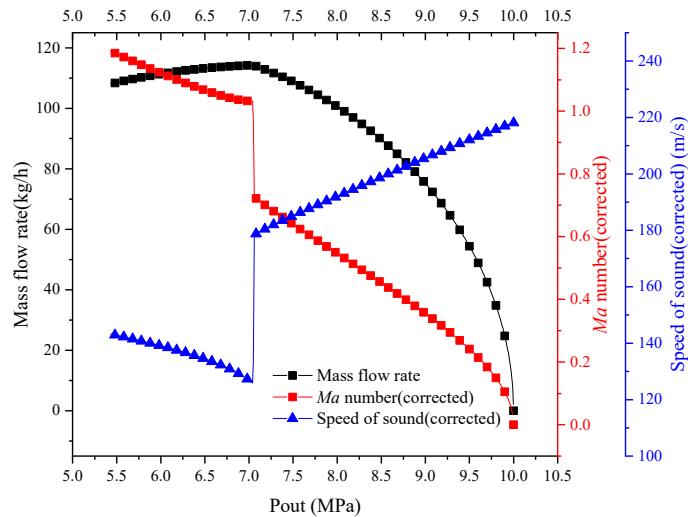


Figure 13. The curve of sealing performance of the round hole calculated by the corrected 1-D method.

4. Results and Discussion

This paper investigates three types of labyrinth, namely round-hole, see-through, and staggered labyrinths. Firstly, existing experimental data are compared to verify the accuracy and applicability of the 1-D method proposed in this paper on the labyrinths with different sealing structures which are summarized in Table 6. Secondly, the influence of different sealing structure on the sealing effect is studied by using the 1-D method, and the law of designing the sealing structure is analyzed in advance.

Notably, all the experiments are conducted at static conditions and the correlations in the 1-D method are ignored the influence of swirl effect which may destroy the conservation of total enthalpy. The critical velocity ratio of $u/U = 1.0$ was introduced by Scherer [23] and Paolillo [24] in which u is the axial velocity and U is the tangential velocity of the high-speed shaft. This was verified by Jun Li [25] through the experimental and numerical study in which a rotational influence on the leakage coefficient does not appear when the criterion ($u/U < 1$) is satisfied. In addition, in the study of Waschka, it was argued that shaft rotation has a negligible effect on labyrinth seal leakage when the local Re number is above 10^4 [26]. For the Re number of SCO_2 flow in labyrinth is much higher than that of air, and the criterion ($u/U < 1$) proposed based on the study of air labyrinth seals may be too strict for SCO_2 labyrinth seals. It is recommended to discuss this further in the future work. Conservatively, the criterion ($u/U < 1$) should be carefully checked when the 1-D method was used to calculate the leakage of high-speed SCO_2 labyrinth seals at this stage.

Table 7. The experiment details of different labyrinth seals compared in this paper.

	Seal Type	Seal Structure	Outlet Condition	Outlet Phase	Re Number
Fan et al.	Round hole	$w = 5 \text{ mm}$, $c = 1 \text{ mm}$, $Z = 1$	Critical	Two-phase	$>10^6$
Yuan et al.	See-through	$w = 1.27 \text{ mm}$, $c = 0.105 \text{ mm}$, $s = 1.27 \text{ mm}$, $h = 0.88 \text{ mm}$, $r = 1.5 \text{ mm}$, $Z = 2$	Critical & Non-critical	Gas & Two-phase	$>10^5$
Zhu et al.	Stepped staggered	$w = 0.3 \text{ mm}$, $c = 0.14 \text{ mm}$, $h = 2 \text{ mm}$, $s = 2 \text{ mm}$, $Z = 4$	Critical	Two-phase	$>10^5$

4.1. Verification of 1-D Computation Method

4.1.1. Round Hole Labyrinth Seal

As expected for the experimental results of different structures of the single round hole used in Section 3.1.2, Fan et al. also presented the detail results of two-phase critical flow corresponding to different inlet temperatures (50–100 °C) and inlet pressure (8 and 10 MPa) respectively, in which the backpressure maintains atmospheric pressure [17]. Table 4 shows the structure of the single round hole.

Before using the 1-D method to calculate the single round hole, the criterion, $Re > 1 \times 10^5$, must be checked. Figure 14 shows the local Re number of critical flows in a single round hole under different inlet conditions, which is over 10^6 .

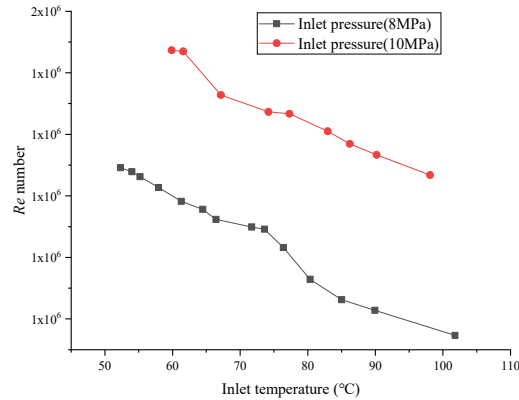


Figure 14. The local Re number of outlet flow under different inlet conditions in Fan’s experiment.

The experimental conditions are suitable for using the 1-D method with critical discharge flow coefficient and the two-phase model of the modified speed of sound. The comparison of calculation results is shown in the Figure 15. Clearly, the 1-D method is highly accurate for different inlet temperatures and pressures, and the calculation error of the 1-D method is within 5%. The comparison indicates that the 1-D method can achieve highly accurate results under two-phase critical flow conditions on the one hand, and on the other hand, the hypothesis of the Re number is verified to some extent.

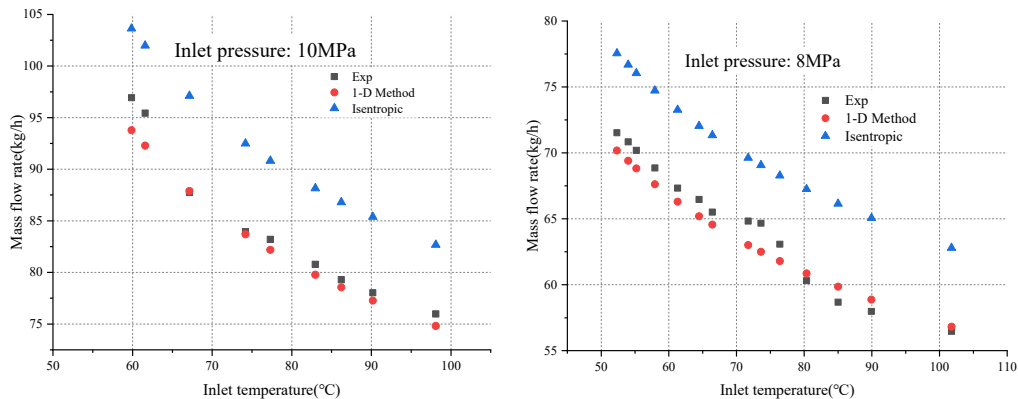


Figure 15. The comparison of the 1-D method, isentropic model and Fan’s experimental results with different inlet temperature and pressure (10 MPa-left and 8 MPa-right).

4.1.2. See-through Labyrinth Seal

Yuan et al. were the first to experiment on the SCO₂ see-through labyrinth seal which obtained a complete curve of sealing performance and provided the detailed experimental data and also carried out numerical simulation study using OpenFOAM [5]. The structure parameter of see-through labyrinth seal used in the experiment is described in Figure 5 and Table 7. The inlet pressure is 10 MPa and the inlet temperature is 318.98 K.

Figure 16 is the local Re number at computation site $n = 1.5$ under different backpressure. The clearance of Yuan’s labyrinth is over 10 times smaller than that of Kim’s round hole labyrinth seal, which causes the local Re number in Yuan’s experiment to be slightly higher than 10⁵. The critical pressure of Yuan’s is about 0.6. When the pressure ratio is less than 0.6, the leakage flow is under critical condition and the local Ma = 1, which means that the leakage flow basically keeps unchanged. And then, the local Re number has little change. However, as the pressure ratio is more than 0.6, the leakage flow is under a non-critical condition, and the local Ma decreases as the pressure ratio increases, which leads to the rapid decrease of Re number.

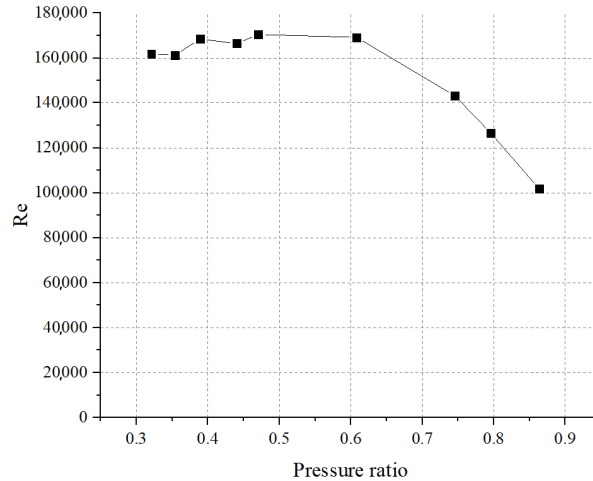


Figure 16. The local Re number at computation site $n = 1.5$ in Yuan’s experiment.

As the backpressure is below 6 MPa, the leakage flow at the outlet may be the two-phase critical flow. As is shown in Figure 17, it can be found that the results of the 1-D method are most consistent with the experiment and the relative error is less than 2% in single-phase and non-critical regions and attain a higher accuracy in the two-phase and critical regions where the relative error is less than 1%.

The traditional computation formulas such as Martin’s formula, Stodola’s formula, Egli’s formula, and Vermes’s formula are included to calculate the see-through labyrinth seal performance curve under the same inlet condition (10 MPa, 318.98 K). The Martin’s formula shows the greatest computational error, because It ignores the kinetic energy transport effect and assumes an isothermal process, which is very different from the actual sealing process. From the perspective of the theory itself, the traditional computation formulas are essentially zero-dimensional equations, and are difficult to surpass the 1-D computational method proposed in this paper in terms of accuracy and applicability.

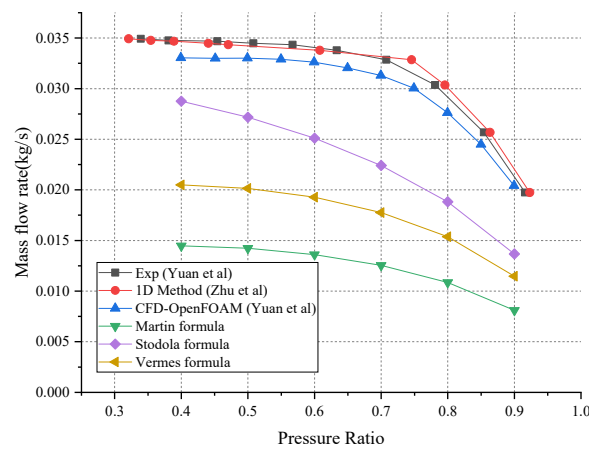


Figure 17. The comparison of SCO_2 see-through labyrinth seal performance curve (based on different methods).

4.1.3. Stepped-Staggered Labyrinth Seal

Our research team developed a stepped-staggered labyrinth seal as the shaft end seal of the SCO₂ centrifugal compressor, which may have better seal performance than the see-through labyrinth seal and avoid the assembly problem of the traditional axial staggered labyrinth seal. The structure and the assembly parts of the stepped staggered labyrinth seal is shown in Figure 18, and the experimental tests under the SCO₂ inlet condition have been completed recently.

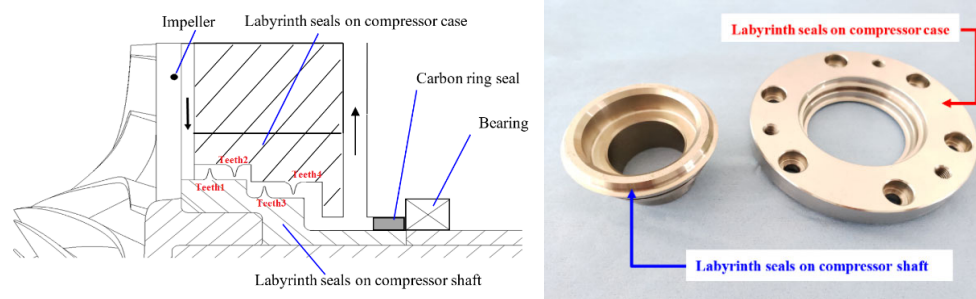


Figure 18. The stepped staggered labyrinth seal used in the SCO₂ centrifugal compressor.

The compressor performance test loop is used to test the stepped-staggered labyrinth seal. To improve the experiment reliability, the sealing experiment is conducted under steady state inlet conditions and the size of clearance and diameter at different sealing teeth is measured to ensure the accuracy of structure parameters used in the 1-D method. The measured results of the sealing structure are listed in Table 8.

Table 8. The measured results of the sealing structure.

	Teeth 1	Teeth 2	Teeth 3	Teeth 4
Sealing clearance (mm)	0.132	0.131	0.129	0.128
Sealing diameter (mm)	53.95	49.97	47.98	44.04

The experiment used a 1.5 m³ high-pressure tank as the gas supply and the set temperature and pressure sensor were close to the compressor inlet to measure the inlet upstream condition of the labyrinth seal. Figure 19 shows the inlet condition of the test, and it can be found that the inlet temperature basically keep unchanged at 39.2 °C and the inlet pressure decreases from 8.01 to 7.88 MPa.

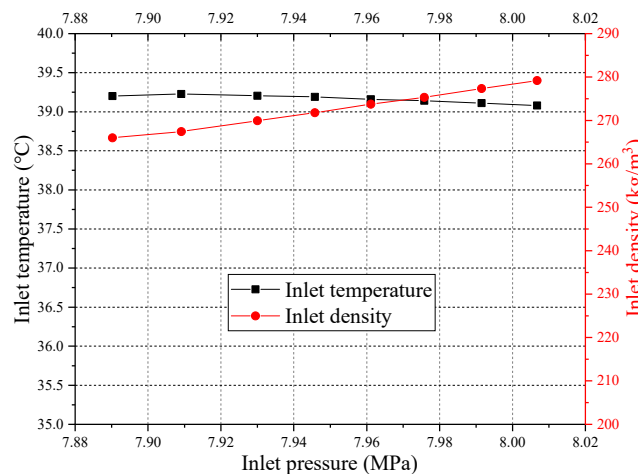


Figure 19. The inlet condition of the stepped staggered labyrinth seal test.

In the discussion of the round hole and see-through labyrinth seal, the local Re number is analyzed firstly, and it is shown that the local Re satisfy the criterion ($Re > 10^5$), and it may have no influence on the calculation of 1-D computation. Figure 20 shows the local Re numbers at different sealing teeth; the minimum and maximum values occur at the first and last teeth, respectively, and they are both larger than 10^5 .

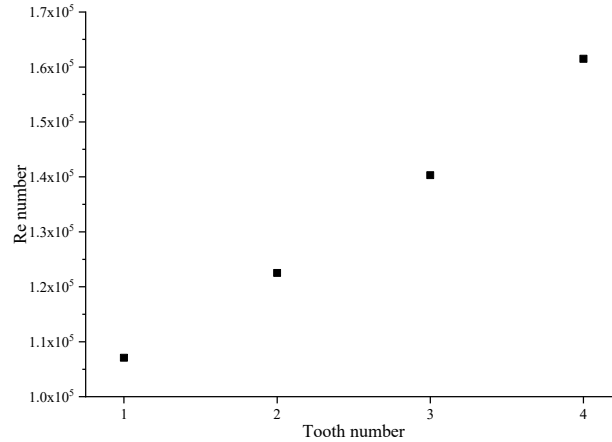


Figure 20. The local Re number at different teeth.

According to the inlet condition of the test, it can be inferred that the critical pressure P_c is about 5 MPa, and the backpressure of the experiment is atmospheric pressure, which means that the outlet status is critical two-phase flow. From Figure 21, the results of the 1-D method are consistent with the test results.

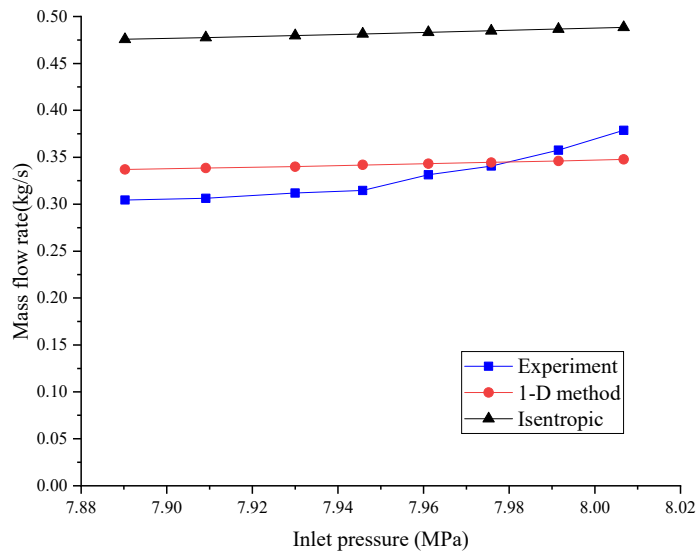


Figure 21. The comparison of 1-D method, isentropic model, experimental results.

4.2. Sealing Efficiency of SCO_2 Labyrinth Seal

The 1-D method has been proved have high accuracy for different kinds of labyrinth seals in Section 4.1. Owing to the modified computational method of speed of sound, the 1-D method is much more accurate in calculating the two-phase critical sealing condition. So, it is accurate and convenient to discuss the design rules of the SCO_2 labyrinth seal using the 1-D method. Generally, it is more appropriate to define a nondimensional parameter to investigate the sealing rules, and the seal

leakage $G_{isentropic}$ calculated by the isentropic flow model mentioned by Sandeep is the maximum computational leakage under a certain condition [18], and then sealing efficiency η_{seal} can be defined as Equation (20).

$$\eta_{seal} = \left(1 - \frac{G}{G_{isentropic}} \right) \times 100\% \quad (20)$$

4.2.1. Effect of Pressure Ratio

Using the curve of sealing performance of see-through labyrinth in Section 4.1.2 to investigate the effect of pressure ratio on sealing efficiency. As is shown in Figure 22, the sealing efficiency increases with an increase in pressure ratio in general. The sealing efficiency increases slowly when the pressure ratio is far from the critical pressure and decreases rapidly when the outlet pressure is close to the atmospheric pressure, indicating that a much more complex sealing structure at the critical outlet may be required to achieve the same sealing effect.

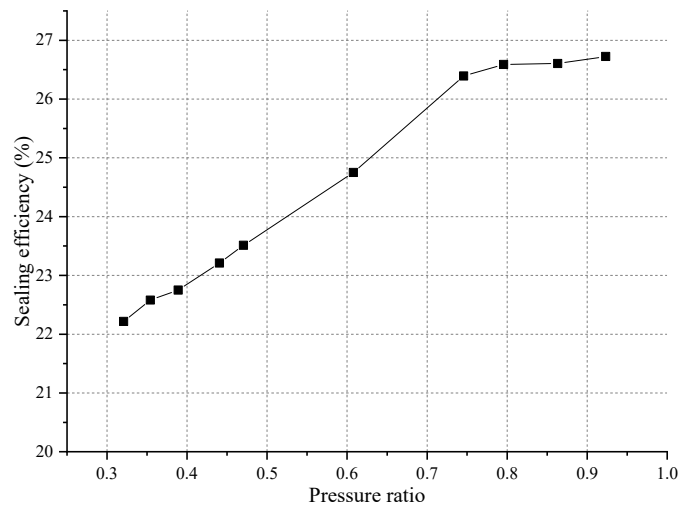


Figure 22. The effect of pressure ratio on sealing efficiency.

4.2.2. Effect of Inlet Condition

Given different inlet pressure and temperature, the variation curve of sealing efficiency for SCO_2 two-teeth see-through labyrinth with different inlet states is shown in Figure 23. Though no phase change is the main characteristics of supercritical fluid, there is a quasi-critical point near which the physical properties change dramatically. Figure 24 shows the sharp change of specific heat C_p near the quasi critical point. For the inlet temperature less than pseudo-critical temperature, it is a liquid-like inlet condition, and by contrast, it is a gas-like inlet condition. Obviously, minimum values of sealing efficiency exist and are located at the inlet temperatures nearby of pseudo-critical temperature. Besides, the “valley effect” of sealing efficiency is weakened as inlet pressure moves farther away from the critical pressure. For the condition of inlet temperature far from quasi-critical temperature, the sealing efficiency is basically unchanged and the liquid-like supercritical inlet condition whose inlet temperature is low enough can be expected to demonstrate higher sealing efficiency than that of the gas-like supercritical inlet condition.

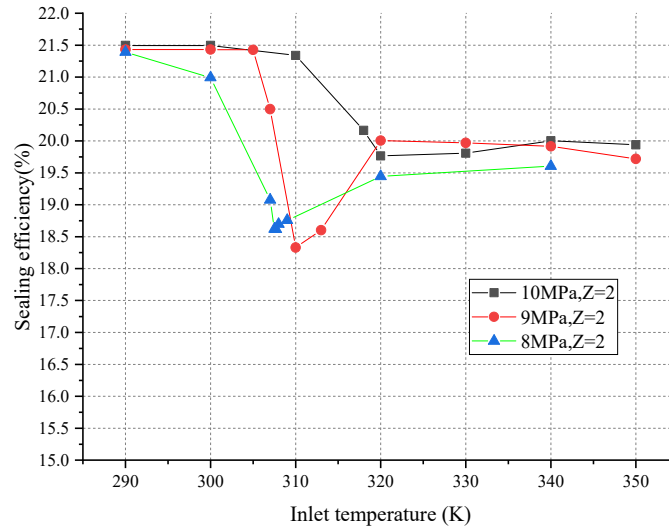


Figure 23. The effect of inlet condition on sealing efficiency.

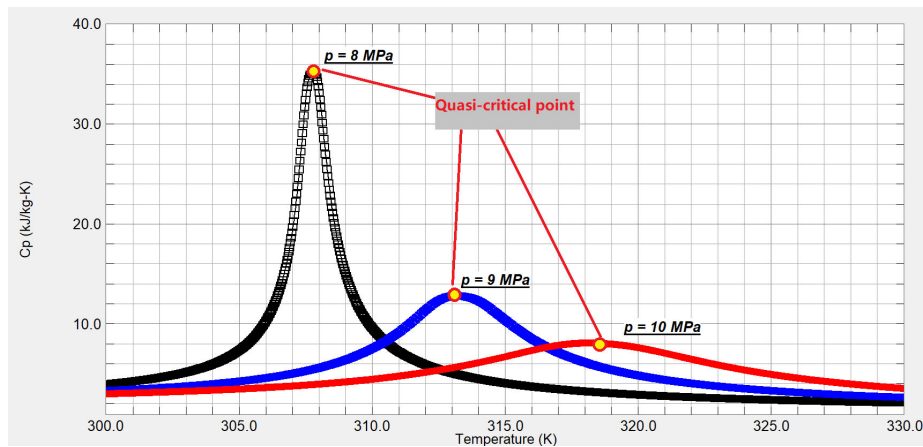


Figure 24. The quasi-critical point of CO_2 .

4.2.3. Effect of Teeth Number Z

Changing the teeth number of see-through labyrinth seal in Table 7, sealing efficiency curves can be plotted, as shown in Figure 25. The sealing efficiency increased dramatically when the teeth number increased from two to five, but as the teeth number continues to increase, the growth rate of the sealing efficiency slows down, which means that it is harder to improve the sealing performance. In addition, the effect of the inlet condition, as discussed in Section 4.2.2, will be magnified when the teeth number increases.

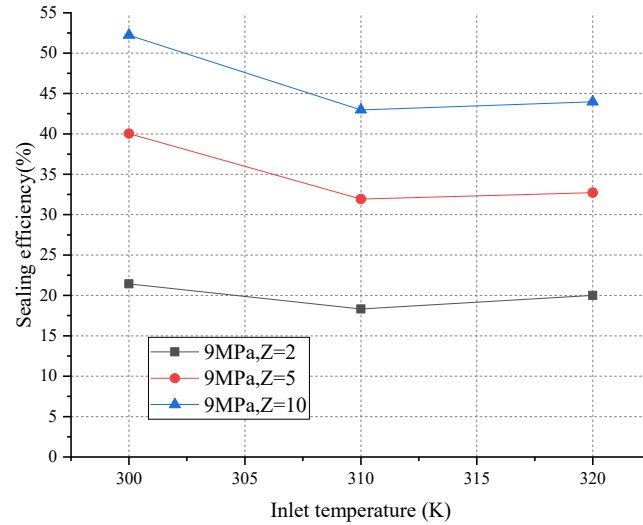


Figure 25. The effect of teeth number Z on sealing efficiency.

4.2.4. Effect of Labyrinth Seal Type

As is discussed in Section 4.2.3, it is inappropriate to pursue higher sealing efficiency by solely increasing the teeth number. So, in this section, the sealing efficiency of see-through and staggered labyrinth seals have been compared in Figure 26. The staggered labyrinth improves sealing efficiency by over 22% for the inlet condition of gas-like SCO_2 and 10% for the inlet condition of liquid-like SCO_2 . Remarkably, the staggered labyrinth seal has a greater advantage on the inlet condition of gas-like SCO_2 and improved the sealing performance

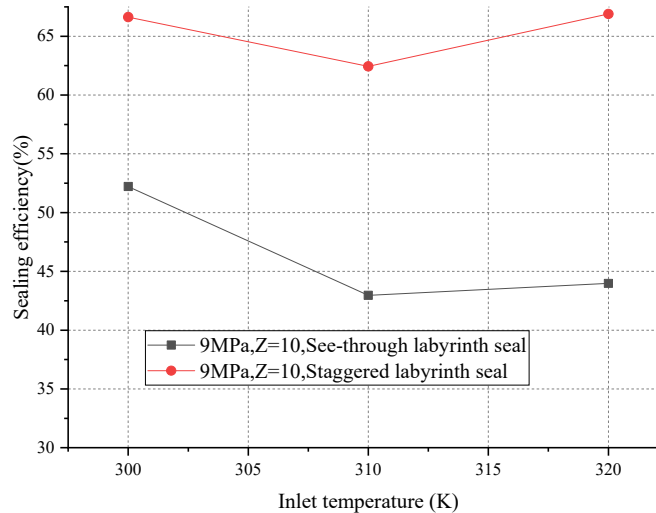


Figure 26. The effect of labyrinth seal type on sealing efficiency.

5. Conclusions

Based on the internal flow characteristics of the labyrinth seal, the 1-D flow hypothesis and the thermodynamic process hypothesis are presented. The 1-D computation method of the labyrinth seal suitable for a real fluid (including a two-phase flow) is proposed.

The SCO_2 sealing flow has the Re number that is two orders of magnitude higher than that of air, and is turbulent flow. The flow discharge coefficient is obviously larger. At the sealing chamber, the kinetic energy transport effect of the supercritical CO_2 working fluid is much more obvious, and the residual kinetic energy coefficient is larger. The influence of Re number on characteristic parameters is assumed to be negligible under the condition $10^5 < Re < 10^7$. Based on the experimental,

numerical results, and traditional theory, the experimental correlation discharge coefficient C and the residual kinetic energy coefficient θ used in SCO_2 labyrinth seals are proposed. The two-phase critical flow was studied, and it is not suitable to use the a_v and a_l in the NIST model to calculate the speed of sound of the two-phase flow in the labyrinth seal, which leads to computational error in the calculation of two-phase critical flow. The speed of sound of two-phase flow is corrected and the problem of critical flow Ma number is perfectly solved.

In this paper, to verify the validity of 1-D method, the results of three types of labyrinths including round-hole, see-through and staggered labyrinth seals are compared, which shows that the computational results of 1-D method are consistent with the experimental results for different types of labyrinth seals and under different inlet conditions, and it is also proven that the flow discharge coefficient and kinetic residual coefficient of 1-D method may not be affected by Re number ($Re > 10^5$) to some extent.

The 1-D method has been used to discuss the influence of various factors on the sealing performance, and the conclusions are as follows:

- The sealing efficiency increases as the pressure ratio increases and increases slowly when the pressure ratio is far from the critical pressure.
- The minimum values of the sealing efficiency exist and are at the inlet temperatures near the pseudo-critical temperature.
- As the teeth number continues to increase, the growth rate of the sealing efficiency slows down.
- The staggered labyrinth seal has more advantages on the inlet condition of gas-like SCO_2 improving the sealing efficiency by 22% compared with the see-through labyrinth seal.

Author Contributions: Conceptualization, Y.Z. and Y.J.; Methodology, Y.Z.; Software, Y.Z.; Validation, Y.Z., Y.G. and H.C.; Investigation, Y.Z.; Writing-Original Draft Preparation, Y. Z.; Writing-Review & Editing, Y.J. and C.G.; Project Administration & Funding Acquisition, Y.J. and S.L. All authors have read and agreed to the published version of the manuscript.

Funding: This research received no external funding or This research was funded by the Strategic Priority Research Program of the Chinese Academy of Sciences, grant number [XDA21010201]. And the APC was funded by Major Special Programs of Science and Technology in Hebei Province (20284502Z) and Industrial Innovation and Entrepreneurship Team Project of Hebei Province (205A4501D).

Conflicts of Interest: The authors declared that there is no conflict of interest.

Nomenclature and Units

Abbreviation

1-D	one-dimensional
CFD	computational fluid dynamics
SCO_2	Supercritical CO_2
C	flow discharge coefficient
Z	teeth number
P	pressure, MPa
T	temperature, K
R	ideal gas constant, J/(mol·kg)
G	mass flux, kg/(m ² ·s)
\dot{m}	mass flow rate, kg/s
h	enthalpy, J/kg
h	the height of sealing chamber, mm
s	entropy, kJ/(kg·K)
A	cross section area, m ²
n	the computational site
k	unit kinetic energy, m ² /s ²
u	flow velocity, m/s
l	characteristic length, m
w	characteristic length, m

c	tooth clearance, m
δP	pressure difference, MPa
δG	iterative error, kg/s
Re	Reynolds number
Ma	Mach number

Greek symbol

ρ	density kg/m ³
μ	dynamic viscosity, Pa·s
θ	residual kinetic energy coefficient
ν	specific volume, m ³ /kg
λ	adiabatic exponent
γ	carry-over coefficient
β	expansion angle, °
η	sealing efficiency, %

Subscription

P_0	inlet pressure, MPa
P_{out}	out pressure, Mpa
P_c	the critical pressure of flow, Mpa
h_0	total enthalpy, kJ/k
h_{00}	inlet total enthalpy, kJ/k
\dot{m}_{00}	inlet mass flow rate, kg/s

References

1. Brun, K.; Friedman, P.; Dennis, R. *Fundamentals and Applications of SCO₂ (sCO₂) Based Power Cycles*; Woodhead Publishing: Cambridge, UK, 2017.
2. Persichilli, M.; Kocludis, A.; Zdankiewicz, E. *Supercritical CO₂ Power Cycle Developments and Commercialization: Why sCO₂ Can Displace Steam Ste*; Power-Gen India & Central Asia: New Delhi, India, 2012.
3. Dostal, V.; Driscoll, M.J.; Hejzlar, P. A SCO₂ Cycle for Next Generation Nuclear Reactors. Ph.D. Thesis, Massachusetts Institute of Technology, Department of Nuclear Engineering, Cambridge, MA, USA, 2004.
4. Kim, M.S.; Bae, S.J.; Son, S.; Oh, B.S.; Lee, J.I. Study of critical flow for supercritical CO₂ seal. *Int. J. Heat Mass Transf.* **2019**, *138*, 85–95.
5. Yuan, H.; Pidaparti, S.; Wolf, M.; John, E. Numerical modeling of SCO₂ flow in see-through labyrinth seals. *Nucl. Eng. Des.* **2015**, *293*, 436–446.
6. Wright, S.A.; Radel, R.F.; Vernon, M.E.; Rochau, G.E.; Pickard, P.S. *Operation and Analysis of a Supercritical CO₂ Brayton Cycle*; Sandia Report No SAND2010-0171; Sandia National Laboratories: Livermore, CA, USA, 2010.
7. Zhu, Y.; Jiang, Y.; Liang, S. Numerical study of super-critical carbon dioxide flow in stepped -staggered labyrinth seals. In Proceedings of the 6th International Symposium on Supercritical CO₂ Power Cycles, Pittsburgh, PA, USA, 27–29 March 2018.
8. Zhao, H.; Deng, Q.; Zhang, H.; Feng, Z. The Influence of Tip Clearance on Supercritical CO₂ Centrifugal Compressor Performance. In *ASME Turbo Expo 2015: Turbine Technical Conference and Exposition*; American Society of Mechanical Engineers Digital Collection; American Society of Mechanical Engineers (ASME): New York, NY, USA, 2015.
9. Parsons, C. Stanley Smith Cook. U.S. Patent 1,374,520, 12 April 1921.
10. Parsons, C. The labyrinth packing. *Engineering* **1938**, *165*, 23–82.
11. Becker, E. Stromungsvergange in Ringformigen Spalten. *VDI* **1907**, *51*, 1133–1141.
12. Martin, H.M. Labyrinth Packings. *Engineering* **1908**, *85*, 35–36.
13. Stodola, A. *Steam and Gas Turbines*; McGraw-Hill: New York, NY, USA, 1927; pp. 189–194.
14. Egli, A. The leakage of Steam through Labyrinth Seals. *Trans. ASME* **1935**, *57*, 115–122.
15. Vermes, G. A fluid mechanics approach to the labyrinth seal leakage problem. *J. Eng. Power* **1961**, *83*, 161–169.
16. Zhu, G. Analysis of calculational methods on leakage for labyrinth seals. *Lubr. Eng.* **2006**, *31*, 123–126.
17. Fan, X.; Wang, Y.; Zhou, Y.; Chen, J.; Huang, Y.; Wang, J. Experimental study of supercritical CO₂ leakage behavior from pressurized vessels. *Energy* **2018**, *150*, 342–350.

18. Pidaparti, S.R. A Computational Study on the Leakage of Supercritical Carbon Dioxide through Labyrinth Seals. Master's Thesis, Texas A & M University, College Station, TX, USA, 2013.
19. Lemmon, E.W.; Huber, M.L.; McLinden, M.O. *NIST Standard Reference Database 23: Reference Fluid Thermodynamic and Transport Properties-REFPROP*; Version 9.1; Standard Reference Data Program; National Institute of Standards and Technology: Gaithersburg, MD, USA, 2013.
20. Suryanarayanan, S.; Morrison, G.L. Labyrinth seal discharge coefficient for rectangular cavities. In *ASME 2009 Fluids Engineering Division Summer Meeting*; American Society of Mechanical Engineers Digital Collection; American Society of Mechanical Engineers (ASME): New York, NY, USA, 2009; pp. 99–114.
21. Furuichi, N.; Terao, Y.; Nakao, S.; Fujita, K.; Shibuya, K. Further experiments and investigations for discharge coefficient of ptc 6 flow nozzle in a wide range of reynolds number. *J. Eng. Gas Turbines Power* **2016**, *138*, 041605, doi:10.1115/1.4031310.
22. Suryanarayanan, S.; Morrison, G.L. Effect of tooth height, tooth width and shaft diameter on carry-over coefficient of labyrinth seals. In *ASME Turbo Expo 2009: Power for Land, Sea, and Air*; American Society of Mechanical Engineers Digital Collection; American Society of Mechanical Engineers (ASME): New York, NY, USA, 2009; pp. 1147–1152.
23. Scherer, T.; Waschka, W.; Wittig, S. Numerical Predictions of High-Speed Rotating Labyrinth Seal Performance: Influence of Rotation on Power Dissipation and Temperature Rise. In *International Symposium on Heat Transfer in Turbomachinery*; Begel House Inc.: Danbury, CT, USA, 1994.
24. Paolillo, R.; Moore, S.; Cloud, D.; Glahn, J.A. Impact of Rotational Speed on the Discharge Characteristic of Stepped Labyrinth Seals. In *ASME Turbo Expo 2007: Power for Land, Sea, and Air*; American Society of Mechanical Engineers (ASME): New York, NY, USA, 2007.
25. Li, Z.; Li, J.; Yan, X.; Feng, Z. Effects of Pressure Ratio and Rotational Speed on Leakage Flow and Cavity Pressure in the Staggered Labyrinth Seal. *J. Eng. Gas Turbines Power Trans. ASME* **2011**, *133*, 114503.
26. Waschka, W.; Wittig, S.; Kim, S. Influence of High Rotational Speeds on the Heat Transfer and Discharge Coefficients in Labyrinth Seals. *J. Turbomach.* **1990**, *114*, 462–468.



© 2020 by the authors. Licensee MDPI, Basel, Switzerland. This article is an open access article distributed under the terms and conditions of the Creative Commons Attribution (CC BY) license (<http://creativecommons.org/licenses/by/4.0/>).